HHS Public Access

Author manuscript

Pain. Author manuscript; available in PMC 2018 November 01.

Published in final edited form as:

Pain. 2017 November ; 158(11): 2108–2116. doi:10.1097/j.pain.0000000000000968.

Fully implantable, battery-free wireless optoelectronic devices for spinal optogenetics

Vijay K Samineni[1,2,*], **Jangyeol Yoon**[3,*], **Kaitlyn E Crawford**[3], **Yu Ra Jeong**[4], **Kajanna C McKenzie**[1,2], **Gunchul Shin**[3], **Zhaoqian Xie**[5,6], **Saranya S Sundaram**[1,2], **Yuhang Li**[7], **Min Young Yang**[3], **Jeonghyun Kim**[3,9], **Di Wu**[5,6], **Yeguang Xue**[5], **Xue Feng**[6], **Yonggang Huang**[5], **Aaron D Mickle**[1,2], **Anthony Banks**[3], **Jeong Sook Ha**[4], **Judith P Golden**[1,2], **John A Rogers**[3,8,#], and **Robert W Gereau IV**[1,2,#]

[1]Washington University Pain Center and Department of Anesthesiology, St. Louis, MO, USA

[2]Washington University School of Medicine, St. Louis, MO, USA

[3]Department of Materials Science and Engineering, University of Illinois at Urbana-Champaign, Urbana, Illinois, USA

[4]Department of Chemical and Biological Engineering, Korea University, Seoul, Republic of Korea, KU-KIST Graduate School of Converging Science and Technology, Korea University, Seoul, Republic of Korea

[5]Department of Civil and Environmental Engineering, Mechanical Engineering, Materials Science and Engineering, Northwestern University, Evanston, IL USA

[6]AML, Department of Engineering Mechanics, Center for Mechanics and Materials, Tsien Excellent Education Program, School of Aerospace, Tsinghua University, Beijing, China

[7]Institute of Solid Mechanics, Beihang University (BUAA), Beijing, China

[8]Departments of Materials Science and Engineering, Biomedical Engineering, Chemistry, Mechanical Engineering, Electrical Engineering and Computer Science, and Neurological Surgery; Center for Bio-Integrated Electronics; Simpson Querrey Institute for Nano/biotechnology; Northwestern University, Evanston, IL, USA

Introduction

The advent of optogenetics allows for temporally precise control of neuronal populations with light via targeted expression of light-sensitive proteins, or opsins [5; 12]. Optogenetic approaches are extensively applied in the neuroscience community to interrogate the causal role of neural circuits in mediating various behaviors [1; 3; 10; 14; 15; 23; 28; 31]. While

[#]Corresponding author: Robert W. Gereau IV, Department of Anesthesiology, Washington University School of Medicine, 660 S. Euclid Ave. Campus Box 8054, St. Louis, MO, 63110, gereaur@wustl.edu or John A Rogers, Department of Materials Science and Engineering, Beckman Institute for Advanced Science and Technology, University of Illinois at Urbana-Champaign, Urbana, IL, 61801, Departments of Materials Science and Engineering, Biomedical Engineering, Chemistry, Mechanical Engineering, Electrical Engineering and Computer Science, Neurological Surgery; Center for Bio-Integrated Electronics; Simpson Querrey Institute for Nano/biotechnology, Northwestern University, Evanston, IL 60208,, jrogers@illinois.edu, jrogers@northwestern.edu.

[*]Equal contributions

[9]Present address: Department of Electronics Convergence Engineering, Kwangwoon University, Seoul, Republic of Korea

optogenetics has been widely applied to study brain circuits, its application to studies of spinal circuits has been hindered by limitations of currently available modes of light delivery. Unlike the brain, where the skull provides a bony anchor point to stabilize optic fibers or head stages for wired or battery-powered light sources, the spinal cord presents unique engineering challenges. Previous studies involving optogenetic approaches to study spinal circuits have relied on epidural optic fiber implants and tethering via fiber optic cables to laser or light-emitting diode (LED) light sources [4; 6; 8; 25]. Although this approach is valuable, tethered operation impedes movement, which can induce stress leading to altered behaviors. The development of a wireless light-delivery system compatible with spinal interfacing would allow broad implementation of optogenetic approaches in studies of spinal circuits, where many behavioral paradigms are not possible or are severely confounded by constraints introduced by tethering.

Recent advances in materials science have allowed for the development of ultraminiaturized LEDs, powered and controlled wirelessly and suitable for use as a device implant for optogenetic stimulation of the brain, and the spinal cord [7; 18; 22; 27; 32; 34; 36]. The original embodiments involved operation in RF (radio frequency) bands that demand specialized equipment and expertise, limiting their utility for broad application by the neuroscience community, particularly in challenging anatomical regions such as the spinal cord. We recently reported the development of a new platform that leverages wireless near-field communication (NFC) at frequencies (13.56 MHz) commonly found in commoditized consumer and industrial wireless electronic devices [21; 39]. The resulting technology offers numerous improvements over previous approaches, including increased ease of operation and customization of wireless settings to various cage types and environments, with little sensitivity to the presence of objects or physical obstructions, including environments consisting of metals. The results enable unrestricted wireless activation of the devices, and the simple design enables mass manufacturing using methods adapted from the flexible printed circuit board industry. Here, we present the development of an optoelectronic system that adapts this NFC technology in an optimized flexible form factor designed specifically for implantation in a minimally invasive fashion over the mouse spinal cord for wireless and battery-free optogenetic interrogation of spinal circuits in freely moving animals.

Methods

Fabrication of implants

The overall device dimensions are 10 mm×5 mm×0.2 mm (L×W×thickness). The rectangular coil designated for wireless transmission consists of 7 planar loops with 50 μm pitch. The probe, equipped with a micro-inorganic light emitting diode (μ-ILED; TR2227, Cree Inc. Raleigh, NC), stems inward from the 5 mm side of the coil, has a width of 400 μm, and is positioned centrally within the otherwise open-architecture device. The μ-ILED emits 470 nm blue light and has dimensions of 220 μm×270 μm×50 μm (L×W×thickness). The transmission coil and needle are composed of a copper, polyimide, copper trilayer (Cu/PI/Cu, 18/50/18 μm thickness, Paralux, Dupont, Dover, DE). The top and bottom Cu layers are bridged through the introduction of 3 laser-drilled holes (50 μm in diameter), which are later filled with conductive silver paste. The transmission coil and probe are

defined through standard photolithography techniques, followed by utilization of a UV laser cutting tool (ProtoLaser U4, LKPF, Germany) to remove excess PI. The electronics that support wireless power transfer capabilities include a capacitor (40 pF, 250R05L220GC4T, Murata electronics, Japan), and a Schottky diode (CBDQR0130L-HF, Comchip Technology, Freemont, CA). The aforementioned components, along with the μ-ILED, are affixed to interconnect points through the use of solder paste. Finally, the optoelectronic device is encapsulated with poly(isobutylene) (PIB; ca. 30 μm thickness, BASF, Southfield, MI) followed by poly(dimethylsiloxane) (PDMS; ca. 10 μm thickness, Sylgard 184, Dow, Freeport, TX). Both layers are generally formed by dip-coating (PIB conc. 8% in heptane, PDMS mixed at 10:1 ratio) with respective drying or curing at 70 °C.

Electromagnetic simulations

Finite element analyses (FEA) was used in the electromagnetic simulations to calculate the Q-factor (a parameter that determines the efficiency of wireless power transfer), the resonant frequency and voltage induced by wireless coupling. The simulations were performed using the commercial software ANSYS HFSS (ANSYS HFSS 13 User's guide, Ansys Inc. 2011), in which tetrahedron elements were used in the solution with adaptive meshing convergence. The default adaptive convergence condition, together with a spherical surface (1000 mm in radius) as the radiation boundary, ensured computational accuracy. The PIB and PDMS device encapsulation layers were ignored due to their negligible influence on the simulation results. The material parameters include the relative permittivity (ε_r), relative permeability (μ_r) and conductivity (σ) of the copper, i.e., $\varepsilon r\_{Cu} = 1$, $\mu r\_{Cu} = 0.999991$ and $\sigma_{Cu} = 5.8\times10^7$ S/m.

Spinal cord light attenuation

Adult male mice (8 week old) were anesthetized with ketamine/xylazine and transcardially perfused with NMDG-substituted aCSF containing (in mM) 93 NMDG, 2.5 KCl, 1.25 NaH2PO4, 30 NaHCO3, 20 HEPES, 25 glucose, 5 ascorbic acid, 2 thiourea, 3 Na-pyruvate, 12 N-acetyl-L-cysteine, 10 MgSO4, 0.5 CaCl2 (pH = 7.3). Lumbar (L3–L5) region of the spinal cord was removed. Longitudinal sections of the spinal cord slices at 250–1000 μm thickness were cut using a Vibratome VT1000s (Leica). The attenuation of blue light through spinal cord slices (250–1000 μm) was measured using an optical power meter (PM 100D, Thorlabs) at 10, 20 and 50 mW/mm^2.

Animals and genetic strategy

Adult (20–25 g) male mice were group housed and maintained on a 12 hr:12 hr light:dark cycle (lights on at 7:00 am). All procedures were approved by the Animal Care and Use Committee of Washington University and adhered to NIH guidelines. Experiments were performed on heterozygous TRPV1-cre male mice [29] crossed to homozygous Ai32 mice [26] from Jackson Laboratory carrying floxed stop-ChR2-EGFP gene in the Gt(ROSA)26Sor locus to generate TRPV1-ChR2 mouse line. As controls we used littermate hetrozygous Ai32 mice (Cre negative).

Surgical procedure: Epidural device implantation

Mice were anesthetized under isoflurane anesthesia on an isothermal heating pad. The dorsal surface above the thoracic and lumbar spine were shaved and cleaned by three alternating washes each of 70% (v/v) ethanol and iodine to the skin to reduce the likelihood of infection. A 2 cm midline incision was made on the dorsal surface, exposing the thoracolumbar vertebral transition. The paraspinal muscles were separated, and the dorsal surface of the T13 vertebral bone was scraped clean [13; 17]. Sterile cotton applicators were utilized to control bleeding. A partial laminectomy was made at the landmark level, allowing for centered placement of the μ-ILEDs over the dorsal horn of the L4-L6 spinal cord segment. Prior to implantation of the μ-ILED device, Kwik-Sil silicone elastomer (World Precision Instruments) was applied onto the dura. Cyanoacrylate glue was utilized to secure the μ-ILED device over the vertebrae. The skin was closed using interrupted sutures and mice were treated with buprenorphine for post-operative analgesia. The animals were then allowed to recover on an isothermal pad with access to food and water ad libitum.

Spinal nerve ligation (SNL)

Mice were anesthetized under isoflurane anesthesia on an isothermal heating pad. Paraspinal muscles were bluntly dissected to expose the L5 transverse process. The L5 transverse process was removed to expose the L4 spinal nerve. The L4 spinal nerve was tightly ligated with silk suture (6-0, Ethicon; Cornelia, GA) and the nerve was transected distal to the ligation. The muscle was closed with 6-0 vicryl suture and the skin was closed with staples. The animal was allowed to recover on an isothermal heating pad.

Real-time place aversion (RTPA)

Place aversion was tested in a custom designed plexiglass chamber with a layer of corn cob bedding [36]. Each arm of the two-arm V-maze is 10 cm wide × 30 cm long×10 cm height with a neutral area between the two arms. The signal was generated in one arm only by tethering the designated arm with a double loop antenna. The signal was attenuated to allow for complete local field coverage and precise control of μ-ILED device power within the designated arm. Each mouse was placed in the neutral area of the chamber, and activity was continuously recorded through a video camera for a period of 20 min. “Time-in-chamber” and heat maps were generated for data analysis using Ethovision software (Noldus, Leesburg, VA). The μ-ILED device was instantaneously and automatically switched to the “ON” state each time the mouse entered into the double loop antenna equipped arm. Similarly, the μ-ILED device was automatically switched to the “OFF” state upon exiting the antenna equipped arm. Software and hardware for generating the signal were from NeuroLux, Inc (Champaign, IL).

Spontaneous pain behavior

Each mouse was placed in an individual plexiglass behavioral chamber. Mice were allowed to acclimate for at least 30 min before testing. White noise generators were used to reduce the influence of external noise pollution on testing. To measure spontaneous behaviors, the wireless μ-ILED devices were activated using a signal generator antenna (NeuroLux, Champaign IL). Behavior was recorded through an HD video camera (Sony) for one minute.

Nocifensive behaviors (defined as licking hind paws, vocalizations, or jumping) were quantified post-hoc from the video recordings by investigators blinded to genotype.

Open field behavior

Open field activity was assessed using a VersaMax Animal Activity Monitoring System (AccuScan Instruments, Inc., Columbus, OH) as previously described [30]. Before testing, mice were habituated to the test room in their home cages for 2 h. Sham and implanted mice were then placed in the open field during individual trials and allowed to freely explore after the experimenter exited the room. Open field locomotor activity was assessed by recording photobeam breaks in a chamber (42 cm × 42 cm × 30 cm, L × W × H) for 30 min. Total distance traveled was calculated for the entire chamber as well as a perimeter (outer 8 cm ring) and center (inner 26 cm × 26 cm square) region.

Rotarod

Locomotor activity was measured on an accelerating Rotarod (Ugo Basile, Italy) to study motor coordination and balance after implantation of the epidural stimulators as previously described [30]. Five consecutive acceleration trials were performed with 5 min breaks separating each acceleration trial in sham mice and mice with spinal implants. Investigators were blinded to treatment (sham vs. implant).

Immunohistochemistry

Mice were deeply anesthetized with a ketamine/xylazine and acepromazine cocktail, then transcardially perfused with cold 4% paraformaldehyde in PBS. The lumbar spinal cord was dissected and placed in 30% sucrose in PBS for overnight cryoprotection, then frozen in OCT. Frozen spinal cord was sectioned at 30 μm in a −20 °C cryostat (Leica) and collected directly onto frosted glass slides. Immunohistochemistry was conducted as described previously [36]. Goat anti-CGRP (1:400, AbD Serotec Cat# 1720-9007), rabbit anti-GFP (1:1,000, Life Technologies Cat# A11122), Rabbit Anti-Iba1 (1:300, Wako Chemicals) and mouse anti-GFAP (1:500, Cell Signaling Technologies) antibodies were used. IB4+ labeling was performed using Alexa Fluor 568-conjugated IB4 (1:400, Life Technologies Cat #I21412). Fluorophore-conjugated secondary antibodies (Life Technologies) were used to visualize primary immunostaining: donkey anti-goat AF647 (1:500), donkey anti-rabbit AF488 (1:500), and goat anti-mouse AF647 (1:500). Slides were sealed overnight with Prolong Gold Antifade Mountant with DAPI (Life Technologies). Images from sealed slides were obtained using a Leica SPE confocal microscope, with gain and exposure time constant throughout image groups. Image acquisition and analysis were performed by an investigator blind to the treatment group.

Statistics

Data are expressed as mean ± SEM. The text and figure legends indicate the statistical test that was used for each dataset. Analysis was either by unpaired t-test (two groups) or two-way ANOVA. The criterion for significance was set at $p < 0.05$ a priori. Researchers were blinded to all experimental conditions. Two replicate measurements were performed and averaged in all behavioral assays.

Results

Optoelectronic device layout

The wirelessly powered device presented in this study is simple to operate and can be easily employed using off the shelf materials and components, without the need for highly specialized equipment. These are critical factors that have been largely absent in previous studies of neuronal function within the spinal circuit using wirelessly enabled optogenetic devices. The device, when placed within the boundaries of an external double loop antenna positioned along the cage perimeter, enables inductively coupled wireless power transmission. The Schottky diode, located at the base of the offset probe, efficiently rectifies the incoming RF signal to power the μ-ILED. A capacitor (40 pF), also positioned at the needle base, provides the necessary impedance matching for efficient device operation (Fig. 1A). Overall device flexibility, lightweight construction (ca. 20 mg), and open oblong design with a single μ-ILED tethered centrally at the probe tip allow for easy manipulation and robust operation. During implantation, the optoelectronic system is applied on top of the vertebral column in a manner that allows the offset probe to be inserted into the rostral end of T13 located above the dorsal horn of the L4-L6 spinal cord segment (Figs. 1B, C & D). A representative image of the fully implanted device in the “ON” state in an awake, freely moving mouse is provided in Fig. 1E.

Optoelectronic device function

By comparison to previous work on NFC enabled devices for optogenetic studies of the brain, robust delivery of light at intensities that are invariant across an experimental environment and stability in chronic operation are considerably more challenging for devices that interface with spinal circuitry. Specifically, operation must provide highly uniform illumination on the target tissue irrespective of the physical location of the animal in xyz-space, for periods of several weeks. In the present study, both theoretical and experimental methods were employed to evaluate the light output power (i.e. μ-ILED illumination intensity) at 27 evenly spaced locations within a designated V-maze arm (12 W output power operating at 13.56 MHz). Nine devices were placed on a planar platform at three different heights within the arm: 2.5 cm, 5 cm, and 7.5 cm. Stable, uniform illumination is achieved when the exterior perimeter of the designated arm is fitted with a double loop antenna (12-gauge Cu wire) such that the lower and upper loops are fixed at 2.5 cm and 7.5 cm from the bottom of the cage (Fig. 2A). For measurement consistency, light output power at each of the 27 locations is normalized to the power measured at the central location at the 5 cm height. Results from Finite Elemental Analysis (FEA) agree well (within 10% error) with the experimental findings (Fig. 2B). The overall variation of light output power across the 27 locations is sufficiently low (less than 10% variation).

Mechanical forces, such as those resulting from vertebral movement in a freely moving awake mouse, may induce out of plane bending of the implanted coil. Severe bending could attenuate the light output power, thereby resulting in unstable illumination and/or irreversible damage to the device. To examine such effects, device stability and wireless performance were evaluated under extreme conditions, with the coil bent from a planar state to a cylindrically curved geometry with a radius of 5 mm (Fig. 2C-inset). The maximum

device strain at a 5 mm radius of curvature was determined using FEA to reach ca. 0.3%, significantly less than the 5.0% fracture strain of Cu, the least compliant of the materials in the flexible portions of the device platform (Fig. 2C) [11; 32; 36]. Here, wireless performance is assessed by examination of two components, the Q-factor and the observed resonance frequency. The Q-factor is a unit-less parameter (ratio of induced voltage to supply voltage at a given resonance, denoted as the voltage magnification) that determines the efficiency for wireless power transfer. In the current study the planar device exhibits a Q-factor of ca. 18.7. As the bending radius of the device is increased to 5 mm the Q-factor decreases by a negligible amount, ca. 0.12. Similarly, the resonance frequency, which describes the optimal frequency of operation, also decreased minimally (by only ca. 0.1 MHz) (Fig. 2D), throughout this range of bending. Jointly, these data suggest that reliable operation of the optoelectronic device introduced in this study can be achieved with consistent wireless performance within the range of changes in curvature that can be expected with normal movement in the mouse.

Heat production from the circuitry or LED is a critical concern as significant increases in tissue temperature could lead to alterations in neuronal function or result in cell damage. In our previous studies, we described studies of thermal effects with similar μ-ILED components in related platforms [37]. Here, we performed additional modeling and extensive testing to ensure that heat production by the designs introduced here are reasonable. Infrared imaging (IR; FLIR A655sc) of the device surface is shown in Fig. 2E before and during wireless operation. At an extreme condition, with continuous operation at an output power of 50 mW/mm^2 in air, the maximum temperature increment from baseline was 1.7 °C. To determine heat generation under conditions more relevant to those in the animal, we measured the temperature at the surface of the μ-ILED in the mouse as a function of pulse width of operation at different power levels (10, 20, and 50 mW/mm^2). Measured values are in good agreement with three-dimensional thermal model simulations, as shown in Fig. 2F. Across a relevant range of conditions, the temperature increases are < 0.5 °C, even at 50 mW/mm^2, 20 Hz, with 5–10 msec pulse widths (i.e. maximum conditions). To understand light penetration through the spinal cord, we measured blue light attenuation through longitudinal spinal cord slices (250–1000 μm) at 10, 20 and 50 mW/mm^2. We delivered these varying intensities of light from the dorsal surface, and observed approximately 70% attenuation at depths of 250 μm, ~95% attenuation at 500 μm, and 100% attenuation of light intensity at depths of 750 μm (Fig. 2G).

A key limitation of previously reported RF-powered wireless devices for studies in the spinal cord was short lifetimes (a few days) associated with mechanical damage from forces introduced by implantation into the epidural space and subsequent mechanical deformations due to motions of the animal. Our present design eliminates the need to insert the μ-ILED into the epidural space, eliminating mechanical strain that could contribute to device failure. The bilayer encapsulation, involving polyisobutylene (PIB) and PDMS, is another critically important modification. Specifically, the additional PIB encapsulation resulted in robust operation of devices over more than four weeks, without power degradation. The average *in-vivo* device survival rate was increased from a period of 1–2 days to nearly 3 weeks (n = 8) by the addition of an underlying PIB barrier coating compared to a single outer PDMS layer

(Fig. 2H). An illustration and images of the implantation process for this optoelectronic system are shown in Figs. 1B, 1C.

Optogenetic studies

To demonstrate the applicability of these optoelectronic spinal devices, we implanted the devices above the dura of the lumbar spinal cord of TRPV1-Chr2 mice. Histological studies demonstrate the presence of robust ChR2^{+} (green) expression in the central terminals of primary afferent neurons in lamina I and lamina II of the spinal cord dorsal horn as evidenced by overlap with CGRP and IB4 (Figs. 3A, 3B). To determine whether the implanted optoelectronic spinal devices caused injury or a neuroinflammatory response in the spinal cord, we stained spinal cord sections for GFAP (Glial fibrillary acidic protein), a marker for astrocyte activation and Iba1, a marker for activated microglia. We did not observe activated microglia or proliferating astrocytes in spinal cord sections from implanted mice. In contrast, spinal cord sections from mice with L4 spinal nerve ligation (SNL, as a positive control) showed robust activation of microglia and astrocytes (Figs. 3C-F), consistent with prior reports [20; 35; 44].

We next examined the functionality and tolerability of these devices in freely moving animals. Implanted devices maintained function over several weeks. Mice with implanted spinal devices exhibited no significant difference in locomotor function or coordination in the rotarod test compared to sham-operated controls (Fig. 4A), and did not result in any change in motor activity in the open field (Fig. 4B). Additionally, chronic implantation of devices did not produce any anxiety-like behavior in the open field test (Fig. 4C), an indication that the devices do not cause significant stress in the mice.

To test whether these devices are effective at manipulating activity of spinal circuitry, we implanted spinal devices in TRPV1-ChR2 and control (Cre-negative) littermate mice, and tested whether optically activing TRPV1 afferents in mice would produce nocifensive behaviors. The TRPV1-ChR2 mice harbor both TRPV1-Cre and Ai32 alleles, which results in the expression of ChR2 in TRPV1-lineage neurons, including the vast majority of unmyelinated fibers [29]. Wireless activation of the spinal μ-ILED at 20 Hz (10 ms pulse width) caused increased nocifensive behaviors in TRPV1-ChR2 mice but not in control mice (Fig. 4D). Optical activation of TRPV1-ChR2 spinal afferents consistently produced reversible flinching, hind paw licking, jumping, and vocalization behaviors. To evaluate whether optical activation of TRPV1-ChR2 spinal afferents produced an aversive state, we placed mice in a custom V-maze apparatus where one arm delivered signal to activate the devices (LED-ON) and one arm was inactive (LED-OFF). TRPV1-ChR2^{+ve} mice showed dramatic aversion to the LED-ON arm, whereas control mice did not show any significant preference for either arm, indicating that optogenetically activating TRPV1-ChR2 spinal afferents causes aversion (Figs. 4E, 4F).

Discussion

We report here a fully implantable optoelectronic system based on wireless, near-field power transfer, with a thin and flexible open-architecture designed specifically for optical stimulation of the spinal cord. Compared to previously reported wireless μ-ILED devices,

these systems offer greatly increased versatility and improved durability, which together allow their broad implementation in even long-term studies [32; 36]. The current optoelectronic system is customized with a rectangular shape that allows direct anchoring of the device over the spinal cord rather than implanting into the epidural space, thereby significantly decreasing mechanical stresses on the device compared to previous platforms [36]. The light weight, battery–free operation, small size with open architecture, and offset needle to minimize light dispersion represent the key technical improvements in this system that allow for effective stimulation of spinal circuits. In addition, a new encapsulation material, i.e. PIB, enables survivability in long-term studies.

The low frequency magnetic inductive coupling scheme can be configured for operation at any optical wavelength by proper selection of μ-ILEDs (UV, blue, green, yellow and red), and widely controlled optical output powers to perform optogenetic stimulation and/or inhibition experiments in the spinal cord. For inhibition studies using green μ-ILEDs, where the operational efficiency is comparatively low, continuous illumination could lead to excessive temperature increases at the device/tissue interface. These effects can be minimized through the addition of an encapsulated copper layer at the needle interface to enhance thermal spreading rate along the needle.

Advanced antenna layouts and electronic component configurations can support significant increases in the operating range. Further, due to the versatility in the fabrication procedures, devices may also be customized for application in larger rodent species. The architecture of this current design can be adapted for capabilities in sensing and wireless data transmission by integrating additional recording electrodes or bio-sensors [22], and wireless drug delivery systems [19].

The proof of concept studies we provide here target stimulation of the central terminals of primary afferents as they enter the superficial dorsal horn, and as such require only minimal light penetration. Our light attenuation results suggest that light intensity falls off quickly, reducing by ~70% at 250 μm, ~95% at 500 μm and 100% attenuation of light intensity at depths of 750 μm in the spinal cord. Although light intensity falls off rapidly as it penetrates the spinal cord, prior publications demonstrate that ChR2-dependent photocurrents can be elicited at very low light intensities (e.g. ~0.1 mW/mm^2) [16; 33; 40; 41]. If one assumes 95% light attenuation at 500 μm as we demonstrate here, a light intensity of 2 mW/mm^2 should be adequate to elicit a minimal photocurrent. The devices described here can be set to generate light intensities of 50 mW/mm^2 or more, and thus induction of photocurrents in neurons deep into the dorsal horn should be easily achieved. Of course, the ability to control neuronal firing with such a photocurrent is dependent on a number of factors including the level of opsin expression and the intrinsic properties such as input resistance, resting membrane potential, etc. of any given cell population. Further improvements in light-dependent modulation of cells or circuits deeper in the spinal cord could be achieved using longer wavelength light in combination with red-shifted opsins [9; 24; 43]. The devices we describe here are capable of powerful illumination of ≥ 50 mW/mm^2, and can be fitted with red μ-ILEDs [39]. With these options, and with the added use of newer generation opsins with increased light sensitivity [2; 9; 24; 38; 42; 43], activation of even neurons deep in the dorsal horn should be possible.

Supplementary Material

Refer to Web version on PubMed Central for supplementary material.

References

1. Anderson DJ. Optogenetics, Sex, and Violence in the Brain: Implications for Psychiatry. Biol Psychiat. 2012; 71(12):1081–1089. [PubMed: 22209636]
2. Berndt A, Lee SY, Ramakrishnan C, Deisseroth K. Structure-Guided Transformation of Channelrhodopsin into a Light-Activated Chloride Channel. Science. 2014; 344(6182):420–424. [PubMed: 24763591]
3. Bernstein JG, Boyden ES. Optogenetic tools for analyzing the neural circuits of behavior. Trends Cogn Sci. 2011; 15(12):592–600. [PubMed: 22055387]
4. Bonin RP, Wang F, Desrochers-Couture M, Ga Secka A, Boulanger ME, Cote DC, De Koninck Y. Epidural optogenetics for controlled analgesia. Mol Pain. 2016; 12
5. Boyden ES, Zhang F, Bamberg E, Nagel G, Deisseroth K. Millisecond-timescale, genetically targeted optical control of neural activity. Nat Neurosci. 2005; 8(9):1263–1268. [PubMed: 16116447]
6. Caggiano V, Sur M, Bizzi E. Rostro-caudal inhibition of hindlimb movements in the spinal cord of mice. PLoS One. 2014; 9(6):e100865. [PubMed: 24963653]
7. Canales A, Jia XT, Froriep UP, Koppes RA, Tringides CM, Selvidge J, Lu C, Hou C, Wei L, Fink Y, Anikeeva P. Multifunctional fibers for simultaneous optical, electrical and chemical interrogation of neural circuits in vivo. Nature Biotechnology. 2015; 33(3) 277-+
8. Christensen AJ, Iyer SM, Francois A, Vyas S, Ramakrishnan C, Vesuna S, Deisseroth K, Scherrer G, Delp SL. In Vivo Interrogation of Spinal Mechanosensory Circuits. Cell Rep. 2016; 17(6):1699–1710. [PubMed: 27806306]
9. Chuong AS, Miri ML, Busskamp V, Matthews GAC, Acker LC, Sorensen AT, Young A, Klapoetke NC, Henninger MA, Kodandaramaiah SB, Ogawa M, Ramanlal SB, Bandler RC, Allen BD, Forest CR, Chow BY, Han X, Lin Y, Tye KM, Roska B, Cardin JA, Boyden ES. Noninvasive optical inhibition with a red-shifted microbial rhodopsin. Nature Neuroscience. 2014; 17(8):1123–1129. [PubMed: 24997763]
10. Copits BA, Pullen MY, Gereau RW IV. Spotlight on pain: optogenetic approaches for interrogating somatosensory circuits. Pain. 2016; 157(11):2424–2433. [PubMed: 27340912]
11. Davis, JR. ASM Specialty Handbook: Copper and Copper Alloys. USA: ASM international; 2001.
12. Deisseroth K. Optogenetics: 10 years of microbial opsins in neuroscience. Nat Neurosci. 2015; 18(9):1213–1225. [PubMed: 26308982]
13. Farrar MJ, Bernstein IM, Schlafer DH, Cleland TA, Fetcho JR, Schaffer CB. Chronic in vivo imaging in the mouse spinal cord using an implanted chamber. Nat Methods. 2012; 9(3):297–302. [PubMed: 22266542]
14. Fenno L, Yizhar O, Deisseroth K. The Development and Application of Optogenetics. Annu Rev Neurosci. 2011; 34:389–412. [PubMed: 21692661]
15. Grosenick L, Marshel JH, Deisseroth K. Closed-loop and activity-guided optogenetic control. Neuron. 2015; 86(1):106–139. [PubMed: 25856490]
16. Grossman N, Poher V, Grubb MS, Kennedy GT, Nikolic K, McGovern B, Palmini RB, Gong Z, Drakakis EM, Neil MAA, Dawson MD, Burrone J, Degenaar P. Multi-site optical excitation using ChR2 and micro-LED array. J Neural Eng. 2010; 7(1)
17. Harrison M, O'Brien A, Adams L, Cowin G, Ruitenberg MJ, Sengul G, Watson C. Vertebral landmarks for the identification of spinal cord segments in the mouse. Neuroimage. 2013; 68:22–29. [PubMed: 23246856]
18. Park S Il, Shin G, Banks A, McCall JG, Siuda ER, Schmidt MJ, Chung HU, Noh KN, Mun JGH, Rhodes J, Bruchas MR, Rogers JA. Ultraminiaturized photovoltaic and radio frequency powered optoelectronic systems for wireless optogenetics. J Neural Eng. 2015; 12(5)

19. Jeong JW, McCall JG, Shin G, Zhang YH, Al-Hasani R, Kim M, Li S, Sim JY, Jang KI, Shi Y, Hong DY, Liu YH, Schmitz GP, Xia L, He ZB, Gamble P, Ray WZ, Huang YG, Bruchas MR, Rogers JA. Wireless Optofluidic Systems for Programmable In Vivo Pharmacology and Optogenetics. Cell. 2015; 162(3):662–674. [PubMed: 26189679]
20. Jin SX, Zhuang ZY, Woolf CJ, Ji RR. P38 mitogen-activated protein kinase is activated after a spinal nerve ligation in spinal cord microglia and dorsal root ganglion neurons and contributes to the generation of neuropathic pain. J Neurosci. 2003; 23(10):4017–4022. [PubMed: 12764087]
21. Kim J, Banks A, Xie ZQ, Heo SY, Gutruf P, Lee JW, Xu S, Jang KI, Liu F, Brown G, Choi J, Kim JH, Feng X, Huang YG, Paik U, Rogers JA. Miniaturized Flexible Electronic Systems with Wireless Power and Near-Field Communication Capabilities. Adv Funct Mater. 2015; 25(30): 4761–4767.
22. Kim TI, McCall JG, Jung YH, Huang X, Siuda ER, Li YH, Song JZ, Song YM, Pao HA, Kim RH, Lu CF, Lee SD, Song IS, Shin G, Al-Hasani R, Kim S, Tan MP, Huang YG, Omenetto FG, Rogers JA, Bruchas MR. Injectable, Cellular-Scale Optoelectronics with Applications for Wireless Optogenetics. Science. 2013; 340(6129):211–216. [PubMed: 23580530]
23. Kravitz AV, Kreitzer AC. Optogenetic manipulation of neural circuitry in vivo. Curr Opin Neurobiol. 2011; 21(3):433–439. [PubMed: 21420852]
24. Lin JY, Knutsen PM, Muller A, Kleinfeld D, Tsien RY. ReaChR: a red-shifted variant of channelrhodopsin enables deep transcranial optogenetic excitation. Nature Neuroscience. 2013; 16(10) 1499-+
25. Lu C, Froriep UP, Koppes RA, Canales A, Caggiano V, Selvidge J, Bizzi E, Anikeeva P. Polymer Fiber Probes Enable Optical Control of Spinal Cord and Muscle Function In Vivo. Adv Funct Mater. 2014; 24(42):6594–6600.
26. Madisen L, Mao TY, Koch H, Zhuo JM, Berenyi A, Fujisawa S, Hsu YWA, Garcia AJ, Gu X, Zanella S, Kidney J, Gu H, Mao YM, Hooks BM, Boyden ES, Buzsaki G, Ramirez JM, Jones AR, Svoboda K, Han X, Turner EE, Zeng HK. A toolbox of Cre-dependent optogenetic transgenic mice for light-induced activation and silencing. Nature Neuroscience. 2012; 15(5):793–802. [PubMed: 22446880]
27. McCall JG, Kim TI, Shin G, Huang X, Jung YH, Al-Hasani R, Omenetto FG, Bruchas MR, Rogers JA. Fabrication and application of flexible, multimodal light-emitting devices for wireless optogenetics. Nat Protoc. 2013; 8(12):2413–2428. [PubMed: 24202555]
28. Miesenbock G. The optogenetic catechism. Science. 2009; 326(5951):395–399. [PubMed: 19833960]
29. Mishra SK, Tisel SM, Orestes P, Bhangoo SK, Hoon MA. TRPV1-lineage neurons are required for thermal sensation. EMBO J. 2011; 30(3):582–593. [PubMed: 21139565]
30. Montana MC, Cavallone LF, Stubbert KK, Stefanescu AD, Kharasch ED, Gereau RW IV. The metabotropic glutamate receptor subtype 5 antagonist fenobam is analgesic and has improved in vivo selectivity compared with the prototypical antagonist 2-methyl-6-(phenylethynyl)-pyridine. J Pharmacol Exp Ther. 2009; 330(3):834–843. [PubMed: 19515968]
31. Montgomery KL, Iyer SM, Christensen AJ, Deisseroth K, Delp SL. Beyond the brain: Optogenetic control in the spinal cord and peripheral nervous system. Sci Transl Med. 2016; 8(337)
32. Montgomery KL, Yeh AJ, Ho JS, Tsao V, Mohan Iyer S, Grosenick L, Ferenczi EA, Tanabe Y, Deisseroth K, Delp SL, Poon AS. Wirelessly powered, fully internal optogenetics for brain, spinal and peripheral circuits in mice. Nature methods. 2015; 12(10):969–974. [PubMed: 26280330]
33. Pandarinath C, Carlson ET, Nirenberg S. A system for optically controlling neural circuits with very high spatial and temporal resolution. Proc IEEE Int Symp Bioinformatics Bioeng. 2013; 2013
34. Paralikar K, Cong P, Yizhar O, Fenno LE, Santa W, Nielsen C, Dinsmoor D, Hocken B, Munns GO, Giftakis J, Deisseroth K, Denison T. An Implantable Optical Stimulation Delivery System for Actuating an Excitable Biosubstrate. Ieee J Solid-St Circ. 2011; 46(1):321–332.
35. Park SI, Brenner DS, Shin G, Morgan CD, Copits BA, Chung HU, Pullen MY, Noh KN, Davidson S, Oh SJ, Yoon J, Jang KI, Samineni VK, Norman M, Grajales-Reyes JG, Vogt SK, Sundaram SS, Wilson KM, Ha JS, Xu R, Pan T, Kim TI, Huang Y, Montana MC, Golden JP, Bruchas MR, Gereau RW IV, Rogers JA. Soft, stretchable, fully implantable miniaturized optoelectronic systems for wireless optogenetics. Nat Biotechnol. 2015; 33(12):1280–1286. [PubMed: 26551059]

36. Park SI, Brenner DS, Shin G, Morgan CD, Copits BA, Chung HU, Pullen MY, Noh KN, Davidson S, Oh SJ, Yoon J, Jang KI, Samineni VK, Norman M, Grajales-Reyes JG, Vogt SK, Sundaram SS, Wilson KM, Ha JS, Xu R, Pan T, Kim TI, Huang Y, Montana MC, Golden JP, Bruchas MR, Gereau RW IV, Rogers JA. Soft, stretchable, fully implantable miniaturized optoelectronic systems for wireless optogenetics. Nat Biotechnol. 2015; 33(12):1280–1286. [PubMed: 26551059]

37. Park SI, Shin G, Banks A, McCall JG, Siuda ER, Schmidt MJ, Chung HU, Noh KN, Mun JG, Rhodes J, Bruchas MR, Rogers JA. Ultraminiaturized photovoltaic and radio frequency powered optoelectronic systems for wireless optogenetics. J Neural Eng. 2015; 12(5):056002. [PubMed: 26193450]

38. Rajasethupathy P, Sankaran S, Marshel JH, Kim CK, Ferenczi E, Lee SY, Berndt A, Ramakrishnan C, Jaffe A, Lo M, Liston C, Deisseroth K. Projections from neocortex mediate top-down control of memory retrieval. Nature. 2015; 526(7575):653–659. [PubMed: 26436451]

39. Shin G, Gomez AM, Al-Hasani R, Jeong YR, Kim J, Xie Z, Banks A, Lee SM, Han SY, Yoo CJ, Lee JL, Lee SH, Kurniawan J, Tureb J, Guo Z, Yoon J, Park SI, Bang SY, Nam Y, Walicki MC, Samineni VK, Mickle AD, Lee K, Heo SY, McCall JG, Pan T, Wang L, Feng X, Kim TI, Kim JK, Li Y, Huang Y, Gereau RW IV, Ha JS, Bruchas MR, Rogers JA. Flexible Near-Field Wireless Optoelectronics as Subdermal Implants for Broad Applications in Optogenetics. Neuron. 2017; 93(3):509–521. e503. [PubMed: 28132830]

40. Wang H, Peca J, Matsuzaki M, Matsuzaki K, Noguchi J, Qiu L, Wang D, Zhang F, Boyden E, Deisseroth K, Kasai H, Hall WC, Feng G, Augustine GJ. High-speed mapping of synaptic connectivity using photostimulation in Channelrhodopsin-2 transgenic mice. Proc Natl Acad Sci U S A. 2007; 104(19):8143–8148. [PubMed: 17483470]

41. Weick JP, Johnson MA, Skroch SP, Williams JC, Deisseroth K, Zhang SC. Functional control of transplantable human ESC-derived neurons via optogenetic targeting. Stem Cells. 2010; 28(11): 2008–2016. [PubMed: 20827747]

42. Wietek J, Wiegert JS, Adeishvili N, Schneider F, Watanabe H, Tsunoda SP, Vogt A, Elstner M, Oertner TG, Hegemann P. Conversion of Channelrhodopsin into a Light-Gated Chloride Channel. Science. 2014; 344(6182):409–412. [PubMed: 24674867]

43. Zhang F, Prigge M, Beyriere F, Tsunoda SP, Mattis J, Yizhar O, Hegemann P, Deisseroth K. Red-shifted optogenetic excitation: a tool for fast neural control derived from Volvox carteri. Nature Neuroscience. 2008; 11(6):631–633. [PubMed: 18432196]

44. Zhuang ZY, Gerner P, Woolf CJ, Ji RR. ERK is sequentially activated in neurons, microglia, and astrocytes by spinal nerve ligation and contributes to mechanical allodynia in this neuropathic pain model. Pain. 2005; 114(1–2):149–159. [PubMed: 15733640]

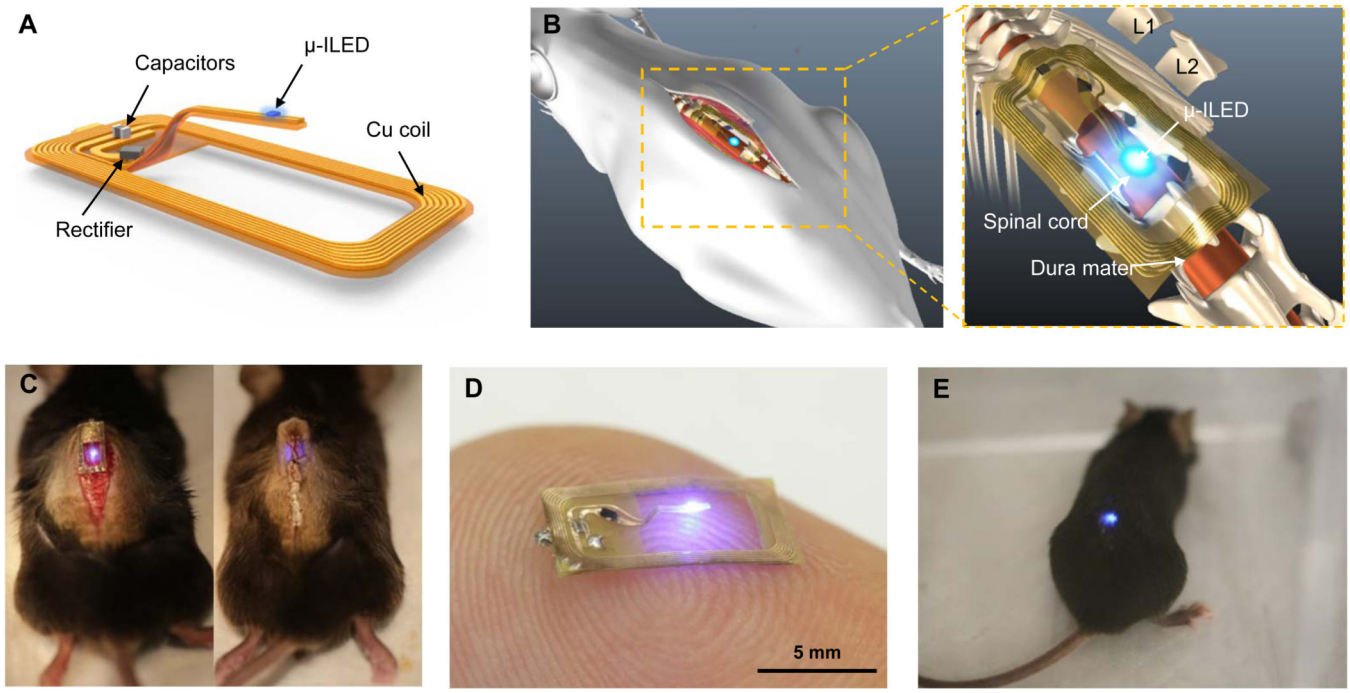

Figure 1. Overall design of the flexible wireless optoelectronic system and the anatomy of the system on the spinal cord

(A) Schematic illustration of the overall system design with open architecture and μ-ILED positioned at the end of the probe stem. (B) Diagram demonstrating the anatomy and location of the optoelectronic system as implanted above the spinal cord. (C) Images of intermittent steps during implantation of the optoelectronic system in the mouse before (left) and after (right) the implantation. (D) Representative image of a device in the 'ON' state while resting atop an index finger. (E) Representative image of an awake, freely moving mouse with the optoelectronic system implanted on the spinal cord.

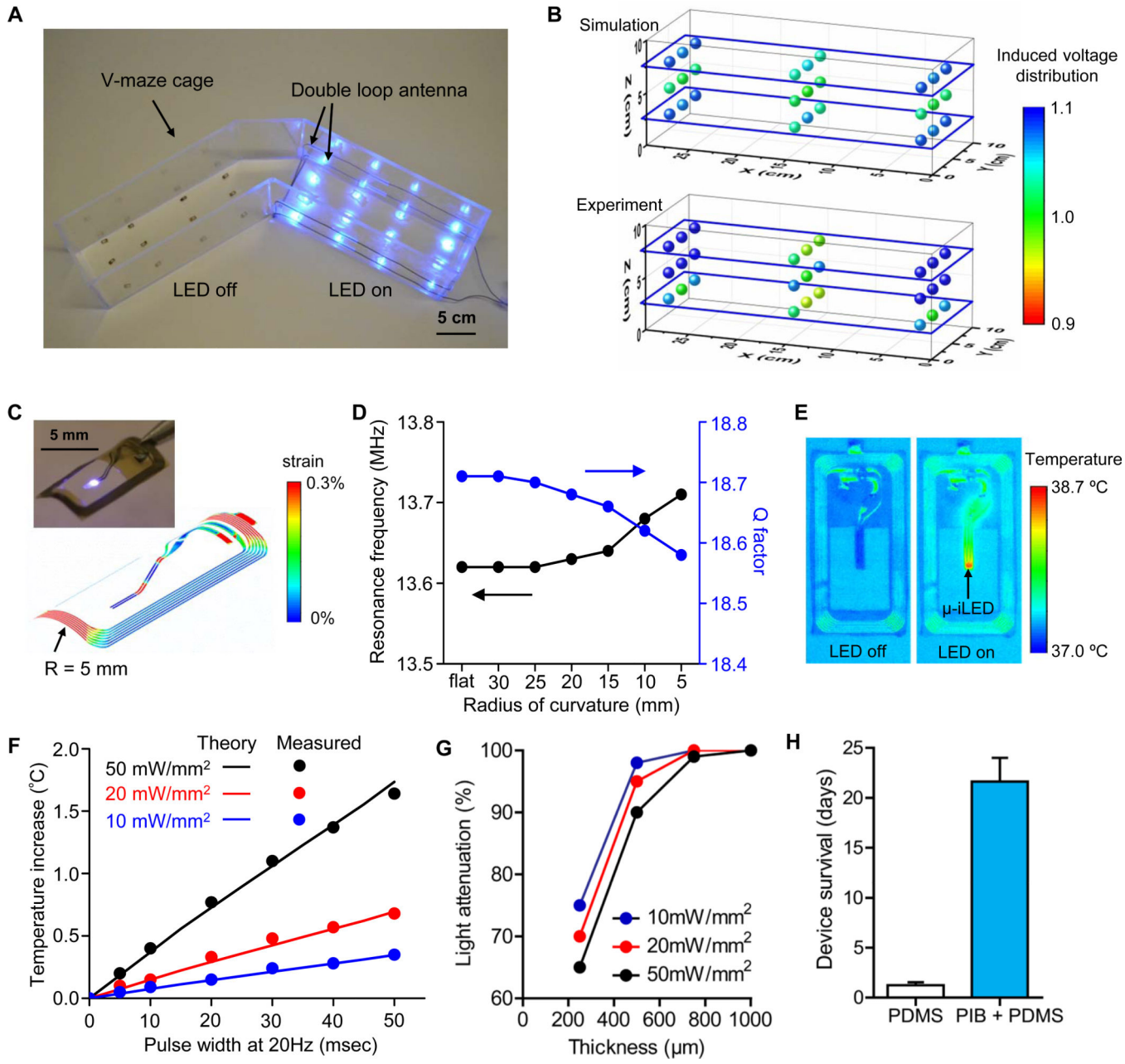

Figure 2. Consistency of power transmission throughout a behavior arena and with mechanical deformation, thermal management, and *in vivo* robustness of the wireless optoelectronic systems

(A) Image of wireless operation of 12 devices in each arm of a V-maze preference arena with the double loop antennas. (B) Simulation (top) and experimental measurement (bottom) of relative output voltage distribution for 27 devices distributed at heights of 2.5 cm, 5 cm, and 7.5 cm from the arena floor. (C) The distribution of the effective strain in the copper coils for the radius of curvatures R = 5 mm. The inset shows a picture of a bent device with a bending radius of 5 mm. (D) The Q factor and resonance frequency obtained by EM simulation for deformed devices with different radii of curvature, from planar to 5 mm. (E) Infrared image of the device surface before and during continuous wireless operation with a

power of 50 mW/mm^2. (F) Temperature change of μ-ILEDs as a function of pulse width of operation at different output powers of 10, 20, and 50 mW/mm^2. (Lines: calculated theoretical values, Symbols: measured experimental values). (G) Blue light attenuation through longitudinal spinal cord slices (250–1000 μm) at 10, 20, and 50 mW/mm^2. (H) Mean (± SEM) days of *in vivo* device survival when encapsulated with a monolayer of PDMS alone (white column) or a bilayer of PIB and PDMS (blue column).

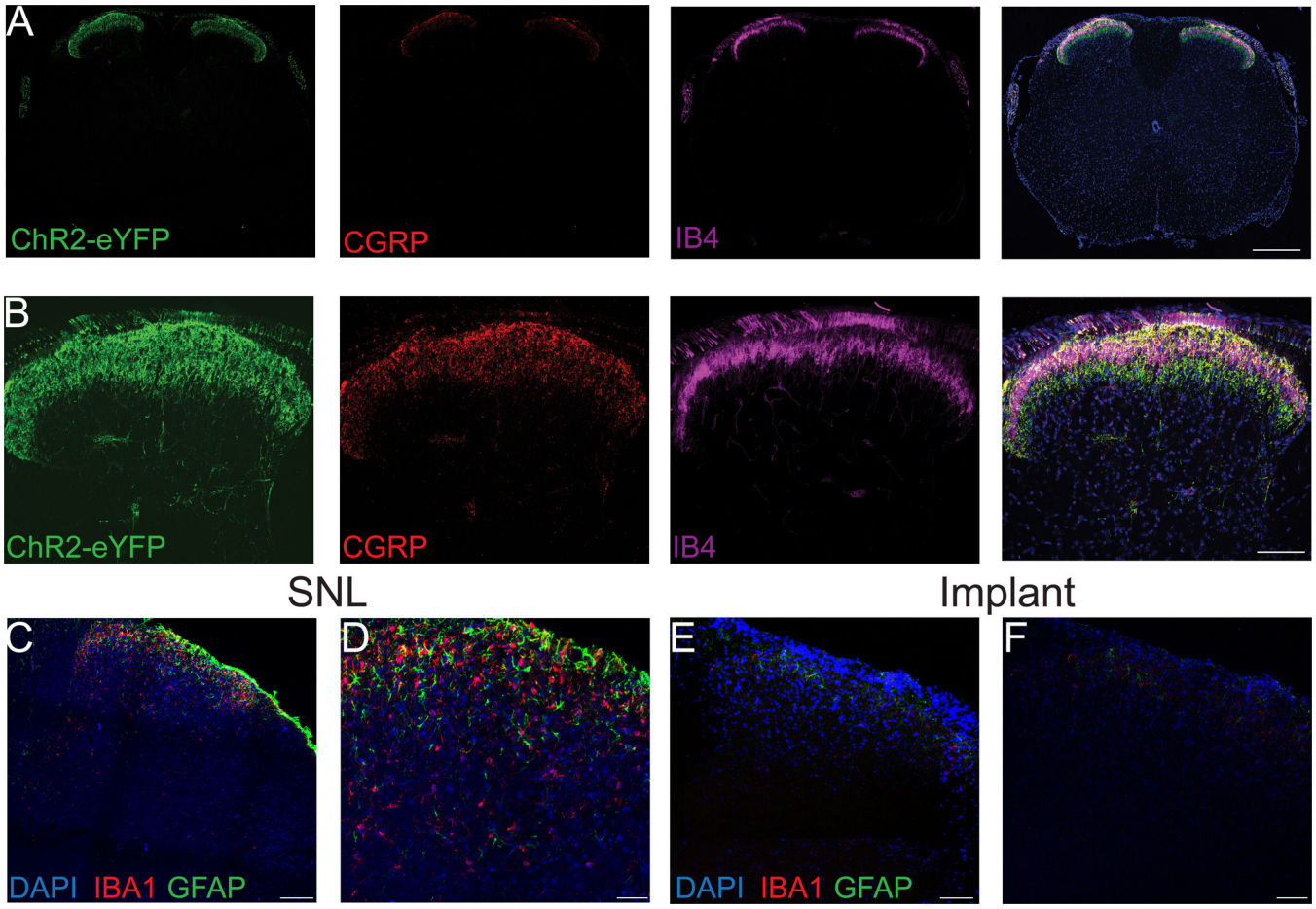

Figure 3. Anatomical and histological characterization of the spinal cord in TRPV1-ChR2 mice

Transverse sections of spinal cord from TRPV1-ChR2 mice at low (A) and high (B) magnification showing ChR2^{+} (green) terminals in the dorsal horn overlapping with CGRP (red) in lamina I and IB4 (magenta) in lamina II. Low magnification and high magnification confocal images of a transverse section of the lumbar spinal cord from a mouse with spinal nerve ligation. Scale bar is 350 μm for low magnification images and 125 μm for high magnification images. (C, D) and from a mouse implanted with the optoelectronic device (E, F) for three weeks. DAPI (blue), GFAP (green) marks reactive astrocytes and Iba1 (red) marks activated microglia. Scale bar is 125 μm for low magnification images and 80 μm for high magnification images.

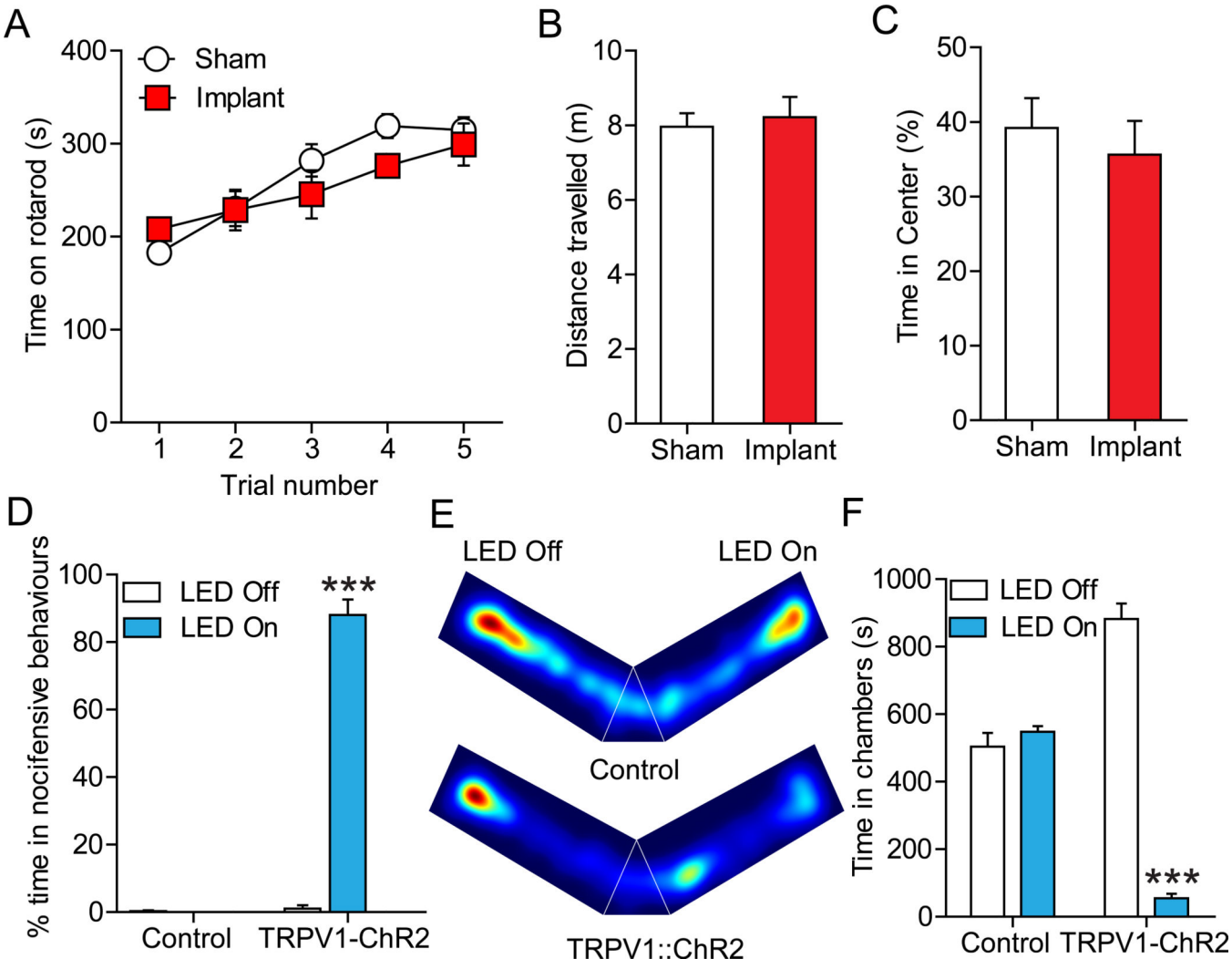

Figure 4. Wireless optical activation of ChR2+ TRPV1 spinal afferents induces pain behaviors and place aversion

(A) Implantation of the spinal optoelectronic device has no effect on motor behavior vs. sham animals in the rotarod test (P = 0.64, n = 6 sham, n = 6 device). (B) Mice with spinal implants did not exhibit any difference in total distance travelled in open field test compared to sham mice (P = 0.56, n = 5 sham, n = 5 device). (C) Implanted mice did not exhibit any difference in time spent in center compared to sham implanted mice in open field test (P = 0.71, n = 5 sham, n = 5 device). (D) Wireless activation of the spinal μ-ILED causes increased nocifensive behaviors (flinching, hind paw licking, jumping and vocalization) in TRPV1-ChR2 mice but not in control (88 vs. 0.25 flinches, P < 0.0001 vs. without illumination n = 6 per group). No other statistical comparisons reach significance. (E) Representative heat maps displaying time spent in a V-maze over a 20 min trial with optical stimulation in the “LED On” arm only for control (top) and TRPV1-ChR2 mice (bottom). (F) TRPV1-ChR2 mice spent significantly less time in stimulation-paired chamber compared with the nonstimulation-paired chamber (54.7 vs. 882.2 s; P < 0.0001, n = 6), whereas control mice did not show any preference (504 vs. 548.3 s; P = 0.665, n = 6). Data

are presented as mean ± SEM. Statistical comparisons were made using two-way ANOVA. ***P < 0.0001.